Radiation Physics and Chemistry 168 (2020) 108600

Contents lists available at ScienceDirect

Radiation Physics and Chemistry

journal homepage: www.elsevier.com/locate/radphyschem

Set up of a gamma spectrometry mobile unit equipped with $LaBr_3(Ce)$ detectors for radioactivity monitoring

E. Prieto[a,*], E. Jabaloyas[a], R. Casanovas[a], C. Rovira[b], M. Salvadó[a]

[a] Unitat de Física Mèdica, Facultat de Medicina i Ciències de la Salut, Universitat Rovira i Virgili, ES-43201, Reus, Tarragona, Spain
[b] SCAR (Servei de Coordinació d'Activitats Radioactives) de la Generalitat de Catalunya, Spain

ARTICLE INFO

Keywords:
Gamma spectrometry
Mobile
Environmental monitoring
Efficiency calibration
Mapping
Nuclear emergency

ABSTRACT

This paper presents the development, calibration and testing of a mobile unit for radioactivity monitoring. A 4 × 4 vehicle was equipped with a GPS and two 2″ × 2″ $LaBr_3(Ce)$ scintillation detectors. It was modelled using MC simulations with the EGS5 code to obtain efficiency curves for different source term scenarios. The attenuation produced by the car structure was determined using MC and experimental measurements. A self-developed software was used to acquire and analyse the gamma spectra. In addition, Minimum Detectable Activity Concentrations were calculated for ^{137}Cs and ^{131}I.

During standard operation, the mobile unit will create a radiological map of Catalonia (Spain), calculating in real time the ambient dose equivalent H*(10) and the activity concentration of natural and anthropogenic radionuclides. After its set up and calibration, the system was tested on the field and provided adequate results. Therefore, the mobile unit is available to assist in the event of a nuclear emergency tracking radioactive plumes and participating in radioisotope mapping surveys. It is also ready to obtain the required data to build the radiological map of Catalonia.

1. Introduction

In Catalonia (Spain) there is an environmental radioactivity surveillance network comprising 26 gamma spectrometry monitors installed all over the region. This network registers and analyses spectra in real time to ensure the radiological quality of the air and land throughout the region and, especially, around the two nuclear power plants that operate in the area.

Recently, the Catalan Government has promoted the development of a new gamma spectrometry mobile unit with two $LaBr_3(Ce)$ scintillation detectors which enables to increase the information provided by the network. Moreover, in the event of a nuclear emergency, the mobile unit will be ready to contribute to track radioactive plumes and to participate in radioisotope mapping surveys.

Traditionally, these mobile units often include various types of radiation detectors, global positioning systems (GPS), meteorological stations and sampling equipment. They have been developed and optimised for nuclear emergencies or radioisotopes surveys (Baeza et al., 2013; Takeishi et al., 2017; Kock, 2010).

However, the objective of the gamma spectrometry mobile unit presented in this paper is not only to increase the radiological information during a nuclear emergency, but also to create a radiological map of Catalonia. This radiological map aims to provide data of the ambient dose equivalent H*(10) and the activity concentration of isotopes from natural and anthropogenic origin all over the region.

This study describes the equipment implementation, calibration and set up of the mobile unit detectors and software. The software, after automatically stabilising and calibrating the collected spectra, calculates the ambient dose equivalent and the activity concentration in real-time. To do so, we considered different source term geometries and calculated their efficiency curves to obtain the activity concentrations using Monte Carlo simulations. In addition, we calculated the attenuation produced by the car structure to the measurements of volumetric, superficial and point-like sources.

The mobile unit was tested across different regions of Catalonia, obtaining a set of 12000 spectra, which were used to check the different equipment and analysis methods. Its performance was satisfactory and therefore, the mobile unit is ready to be used during a nuclear emergency and to start the measurements required to build the radiological map of Catalonia.

2. Material and methods

The mobile unit consists of a 4 × 4 wheel traction car (Toyota

* Corresponding author.
E-mail address: elena.prieto@urv.cat (E. Prieto).

https://doi.org/10.1016/j.radphyschem.2019.108600
Received 31 July 2019; Received in revised form 28 October 2019; Accepted 20 November 2019
Available online 21 November 2019

Fig. 1. Rear view of the mobile unit with the detectors installed on the roof rack.

Rav4) that is prepared to acquire gamma spectra using two 2″x2″ $LaBr_3$(Ce) scintillation detectors (*BrilLance 380* from Saint Gobain Crystals ®), which were placed inside an hermetically sealed plastic case and mounted on the roof rack of the car at 1.8 m height above the ground. The detectors were positioned parallel to the roof and pointed out to each side of the car. The detectors can shift their position to stick out from the width of the car to widen the field of view reducing the attenuation produced by the car structure. When the car circulates through narrow roads surrounded by trees, the devices can be positioned inwards. All the mechanical devices were set up by Raditel Serveis i Subministraments Tecnològics S.L. The detectors are coupled to digital multichannel analysers (*digiBASE* from ORTEC®) that operate in 1024 channels. The multichannel analysers connect to the portable computer located inside the car cabin by a USB port. The system is set to acquire spectra every 30 s, simultaneously in both detectors (See Fig. 1 and Fig. 2).

2.1. Energy and resolution calibrations

The energy and resolution calibrations were performed using five radioactive point sources (^{214}Am, ^{133}Ba, ^{137}Cs, ^{60}Co and ^{152}Eu) and including peaks of radionuclides from natural origin (^{212}Pb, ^{214}Pb and ^{214}Bi). Additionally, the double peak of ^{138}La arising from the self-contamination of the detector crystal and the associated X-ray peak at low energies were also used. Both calibrations were obtained adjusting a 2nd degree polynomial, as it was found to be the best fit function in a previous study (Casanovas et al., 2012a). To compensate the peak drifts caused mainly by temperature variations, spectra were stabilised using a self-development software that automatically adjusts the position of various reference peaks in each spectrum (Casanovas et al., 2012b).

2.2. Efficiency calculations

The efficiency relates the number of counts obtained by the detector with the activity of a radioactive source. The efficiency depends on the source characteristics (energy, distance, composition, geometry, etc.) and on the detector features (materials, geometry, etc.).

For efficiency calculations, two different scenarios were considered: superficial and volumetric source term distributions. However, to study the attenuation produced by the car structure, an extra scenario of a point-like source at 5 m from the back of the mobile unit was also considered. All efficiencies were determined for one single detector of the mobile unit. When using the infinite source approach, both detectors can be considered as only one with twice the efficiency.

The efficiency calibration was calculated using Monte Carlo simulations with the EGS5 code. The car and the detectors were modelled considering the real dimensions and materials obtained from the

Fig. 2. Interior of the car cabin. A portable computer displays in real time the radiological data and the GPS coordinates of the last measured spectra.

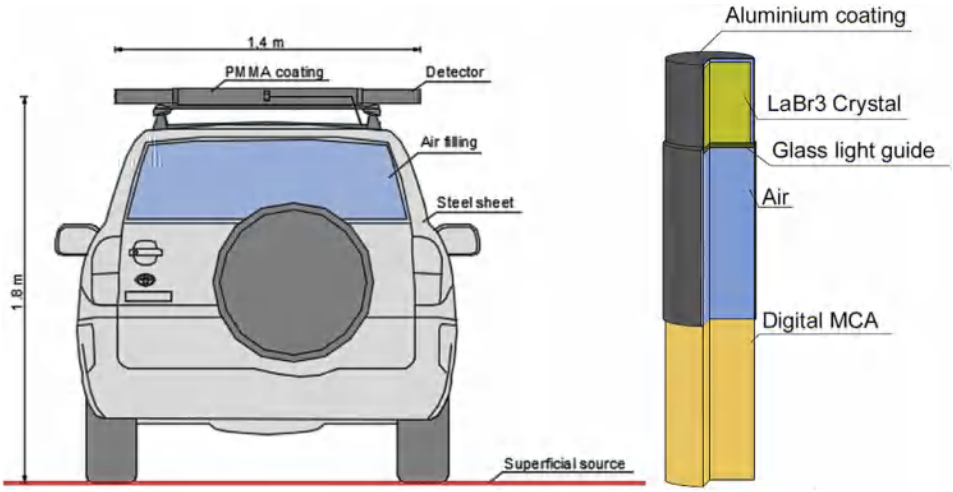

Fig. 3. Models of the mobile unit and the detector used for the efficiency calculations.

technical specifications sheet of both items. The car has a length of 460.5 cm, a width of 184.5 cm and a height of 170.5 cm including the tires. It was considered as a steel structure filled with air. The detectors were modelled with a 2″x2″ cylindrical crystal of $LaBr_3$(Ce) inside an Al case of 0.5 mm of thickness. The space between the case and the crystal was filled with air. A glass light guide was placed adjacently to the crystal. Finally, the photomultiplier tube was modelled as a cylinder of Al and Cu filled with air (see Fig. 3). The density and composition of the materials were taken from Berger et al. (2005).

The code simulated different monoenergetic radiation sources (from 50 to 2000 keV) with a homogenous activity concentration for the three scenarios. The source was modelled as a disk of radius R and as a cylinder of radius R and height H = 2R, for the superficial and volumetric scenarios respectively. The two scenarios are illustrated in red colour in Fig. 4.

The volumetric and superficial efficiencies were calculated using the methodology explained in (Casanovas et al., 2014). First, the efficiency was obtained for different 2R values ranging from 0.0 to 500.0 m, considering a homogenous and monoenergetic source of 661 keV, which corresponds to the ^{137}Cs emission.

Then, the efficiency curves in function of the energy were calculated using 2R = 100 m for the superficial geometry and 2R = 300 m and H = 300 m for the volumetric one. The results were adjusted with the following polynomial equation:

$$\log \varepsilon_x = \sum_{n=0}^{6} a_n (\log E)^n \quad (1)$$

where ε_X is either the volumetric efficiency ε_V or the superficial efficiency ε_S at the gamma-ray energy E and a_n represents the fitting coefficients.

The efficiency that corresponds to a point-like source placed at 5 m from the rear of the mobile unit was also determined and adjusted using Equation (1).

In case that gamma emissions from artificial radionuclides were detected, the developed code is prepared to obtain the activity concentration of any source term distribution.

2.3. Attenuation of the car structure

The car structure affects the measurements obtained by the detectors placed on the rooftop of the mobile unit, since the car acts as a barrier for gamma rays. To measure this effect, the car attenuation was calculated using MC simulations for the volumetric and superficial source term scenarios and experimentally for a point-like source term.

For the volumetric and superficial source term scenarios, the counts due to a ^{137}Cs emission were obtained with and without the car structure. The simulations considered the same parameters used in the efficiency calculations.

For the experimental calculations 5 min spectra were registered using a punctual calibrated source of ^{137}Cs in 23 different positions in front, behind, under and in both sides of the car (see Fig. 5). The measurements were performed twice: with and without the car structure. The mobile unit was parked at the same spot during the spectra registration to avoid variations of natural radiation.

The attenuation parameter is defined as the relation between the

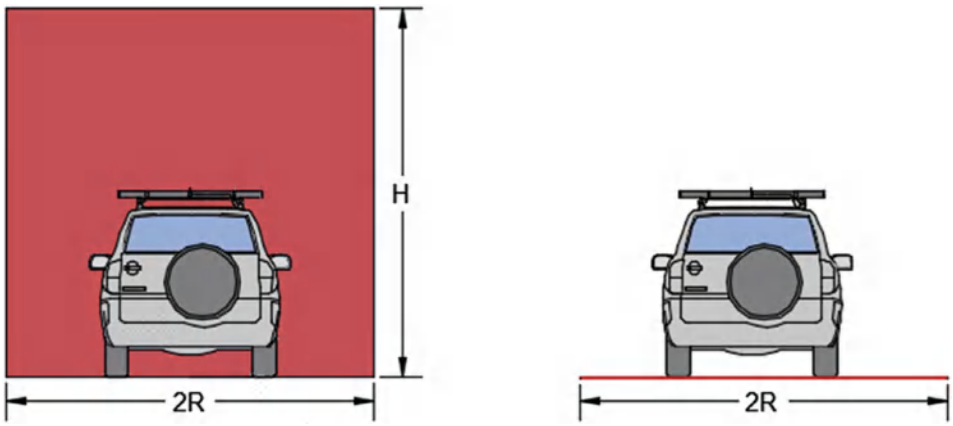

Fig. 4. Volumetric and superficial representation of the source term.

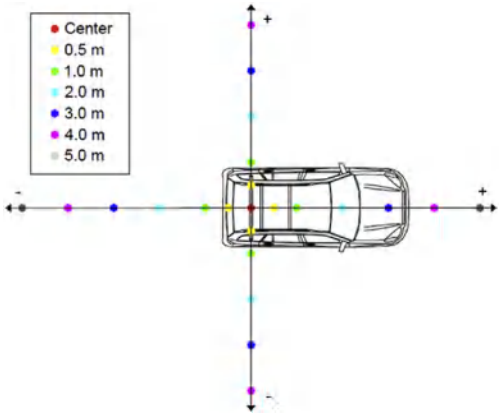

Fig. 5. ^{137}Cs source positions used to measure the car structure attenuation.

measurement obtained with and without the car for a specific source distance. The attenuation percentage was calculated from ^{137}Cs counts obtained in the spectra by:

$$a = \frac{c - c_0}{c_0} \quad (2)$$

Where c is the number of net counts per second (cps) of ^{137}Cs with the car structure and c_0 is the number of net cps without the car. The ^{137}Cs net counts were obtained using the methodology presented later in Section 2.5 Spectral windows method.

The attenuation was measured for both detectors independently. For the longitudinal attenuation a mean value was obtained.

2.4. Ambient dose equivalent H*(10)

Once the spectra are stabilised and calibrated, they can be analysed to obtain the ambient dose equivalent. The ambient dose equivalent is the recommended quantity to assess effective dose in area monitoring and it is defined as the dose that would be produced by the corresponding expanded and aligned field in the ICRU sphere at a 10 mm depth (ICRP: ICRP Publication 103, 2007). The ICRU sphere (ICRU: ICRU Report 39) is a 1 g/cm^3 homogeneous density sphere with a 30 cm diameter. The composition of the sphere is 76.2% O, 11.1% C, 10.1% H and 2.6% N.

The ambient dose equivalent is calculated from the gamma-ray spectra obtained with $LaBr_3$(Ce) detectors using a self-development method that was previously validated (Casanovas et al., 2016). Briefly, the method consists in calculating the fluence of the gamma-ray spectra. Then, it applies conversion factors that obtain the H*(10) ambient dose equivalent from the fluence. The fluence to H*(10) conversion factors were obtained using Monte Carlo simulations with the EGS5 code system.

In the H*(10) calculation study (Casanovas et al., 2016), the H*(10) results for LaBr3(Ce) detectors were found to be inferior to the measurements obtained with a calibrated Geiger Müller tube. Thus, we calibrated the $LaBr_3$(Ce) detector for the mobile unit study. The detector could have been calibrated in a certified laboratory. However, we tried an alternative way using available equipment. To set up the H*(10) calculation methodology for the mobile unit, the obtained ambient dose equivalent was compared and adjusted to the values registered by other calibrated detector systems: a set of thermoluminiscent detectors (TLDs) and a proportional counter. The TLDs used were calibrated for environmental dose measurements and the proportional counter used was a RS04L from BITT Technology, model NPGD 02. The counter detects gamma-rays from 40 keV to 3 MeV and it operates in a 10 nSv/h – 15 mSv/h ambient dose equivalent range with a precision of ± 30% with respect to ^{137}Cs.

The gamma spectrometry detectors of the mobile unit, the TLDs and the proportional counter were placed in an outdoor environment with natural background variations for several days. The spectrometry detectors and the proportional counter obtained data every 10 min.

Then, the mean value of H*(10) obtained from the spectra during the measurement period was rescaled to the H*(10) measurement given by TLDs which were read by a certified laboratory. On the other hand, the relative variations of the H*(10) obtained from spectra were adjusted to the relative variations of the proportional counter fitting a 2nd degree polynomial.

Finally, the method was adapted to the computational capacities of the aboard laptop. The H*(10) calculation process was optimised and mathematically simplified. For example, the 40 conversion factors that were used in the original method were adjusted to a polynomial function in this study. Thus, the computation time for the spectra stabilisation, the energy calibration and the ambient dose equivalent calculation was reduced to less than 1 s.

2.5. Spectral windows method

Gamma spectra are also analysed using another self-developed method that is based on the spectral windows technique (Prieto et al., 2017). This method obtains the activity concentration of a radionuclide from the counts in a spectral window or region of interest (ROI) set around a gamma emission of the studied radionuclide. It corrects for the surplus counts that contribute to a ROI due to close emissions from other radionuclides (overlapping) and for the counts associated to Compton scattering from radionuclides of natural origin.

The target radionuclides are the following natural ones ^{214}Bi, ^{214}Pb, ^{212}Pb and the artificial ones ^{137}Cs and ^{131}I. The activity concentration of the artificial radionuclides is expected to be null during mapping measurements in a normal situation, but it is calculated to trigger an alarm in case of positive detection.

The activity concentration of the target radionuclides was calculated for the different efficiencies: superficial, volumetric and a point-like source.

Additionally, one can calculate the increment of the ambient dose equivalent that corresponds to artificial radionuclides, such as ^{137}Cs, combining the ambient dose equivalent and the spectral windows methods. The explanation of this derived method is focused on the measurement of ^{137}Cs, although it can be applied to any other artificial radionuclide of interest.

To determine the increment of the ambient dose equivalent that corresponds to a detection of ^{137}Cs, we obtained a set of measurements without presence of any artificial radionuclide. Another set of spectra with different amounts of cps from ^{137}Cs was registered placing a point-like source at various distances. Then, the ambient dose equivalent H*(10) was obtained from all the spectra: those that contained different amounts of ^{137}Cs and those without ^{137}Cs. We obtained the increment of the ambient dose equivalent due to ^{137}Cs for all the spectra that contained different amounts of ^{137}Cs subtracting the ambient dose equivalent value of the scenario without ^{137}Cs to those with ^{137}Cs. After that, the spectral windows method was applied to these spectra and the activity concentrations for the three previously calculated efficiencies were determined.

This derived method stablishes a relation between the activity concentration of an artificial radionuclide and the increment to the ambient dose equivalent originated by this activity concentration. A statistical criterion was set to trigger an alarm of a positive detection: the measurements that surpass $\bar{x} + 3.5\sigma$ were considered as a positive detection, where $\bar{x}$ is the mean value for ^{137}Cs activity concentration (which is null in a normal situation) and σ is the standard deviation of a set of measurements without the studied artificial radionuclides.

2.6. MDAC

The Minimum Detectable Activity Concentration (MDAC) of ^{137}Cs

and ^{131}I was calculated after applying the spectral windows technique, as described in (Prieto et al., 2017), for the 30 s measurements of the mobile unit. The calculation of the MDAC considers the subtraction of the intrinsic background of the detector to determine the limit of detection. The limit of detection can be obtained with the standard deviation of a set of activity concentration values calculated using the spectral windows methodology.

The MDAC can be determined as:

$$MDAC = \frac{L_D}{\varepsilon \cdot t \cdot p_\gamma} \quad (3)$$

where the detection limit L_D (with a 95% confidence limit) for a certain ROI is calculated using the expression for the standard deviation of the background (Currie, 1968):

$$L_D = 2.71 + 3.29\sigma_B \quad (4)$$

where σ_B is the standard deviation of the background (laboratory plus the intrinsic background in $LaBr_3$(Ce) detectors) measured in counts in the considered ROI. The width of the ROI is determined for a 95.45% peak area coverage.

2.7. Positioning of the measurements

The mobile unit moves at a maximum speed of 30 km/h and registers a spectrum every 30 s. Each registered spectrum is associated to GPS coordinates. To control the distribution of the acquired spectra, the extension of Catalonia was divided in a 1425 cells grid of 5 × 5 km^2 each. Fig. 6 presents the map of Catalonia with the division cells and an example of the GPS coordinates of some spectra registered in Barcelona. Each marked position (red dots) represents a spectrum registered every 30 s and it displays its corresponding ambient dose equivalent.

2.8. Software

The portable computer placed beside the driver is equipped with a self-developed software. This software places every registered spectrum on the corresponding cell in real time. The 1425 cells of the map of Catalonia are displayed in a different colour, depending on the quantity of registered spectra within each of them. By way of example, Fig. 7 presents the extension of Catalonia divided in square cells in different colours to indicate the spectrum density. The empty cells illustrate the background of the map picture whereas the cells that contain up to 10, 50, 200 or more spectra are drawn in green, yellow, orange and red, respectively.

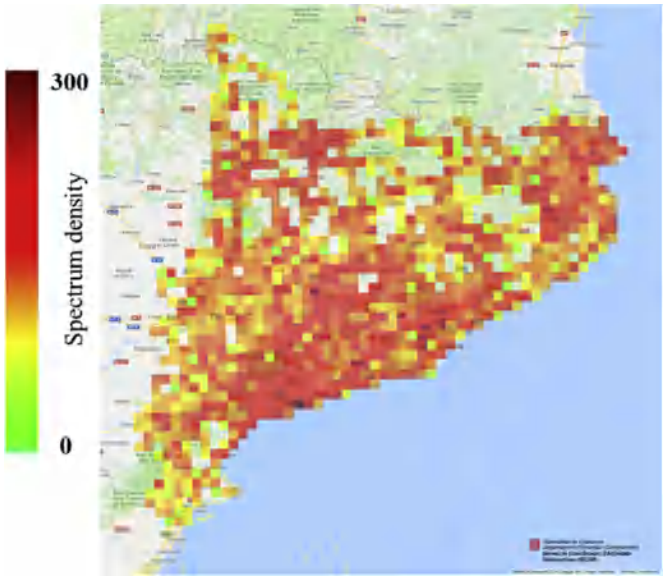

Fig. 7. Colour scale illustrating the spectra density registered within each cell. (For interpretation of the references to colour in this figure legend, the reader is referred to the Web version of this article.)

The number of spectra acquired in each cell depends on various factors. For example, the different shapes of the available paths within a cell, the difficulty of travelling at a constant speed due to traffic or traffic restrictions of the different types of ways (highways, roads, streets..), the number of occasions that the mobile unit travels along the same path to obtain more spectra, etc.

The program also processes the spectra to apply the previously mentioned methodologies: the different calibrations, stabilisation and the calculations of the H*(10) and the activity concentration of some studied isotopes. It presents the obtained ambient dose equivalent H*(10) and the activity concentration of the studied radionuclides in real time. Therefore, when the software obtains unexpectedly high values of the dose equivalent or the activity concentration of a radionuclide, the driver of the car is able to modify the route to acquire more spectra in the suspicious area.

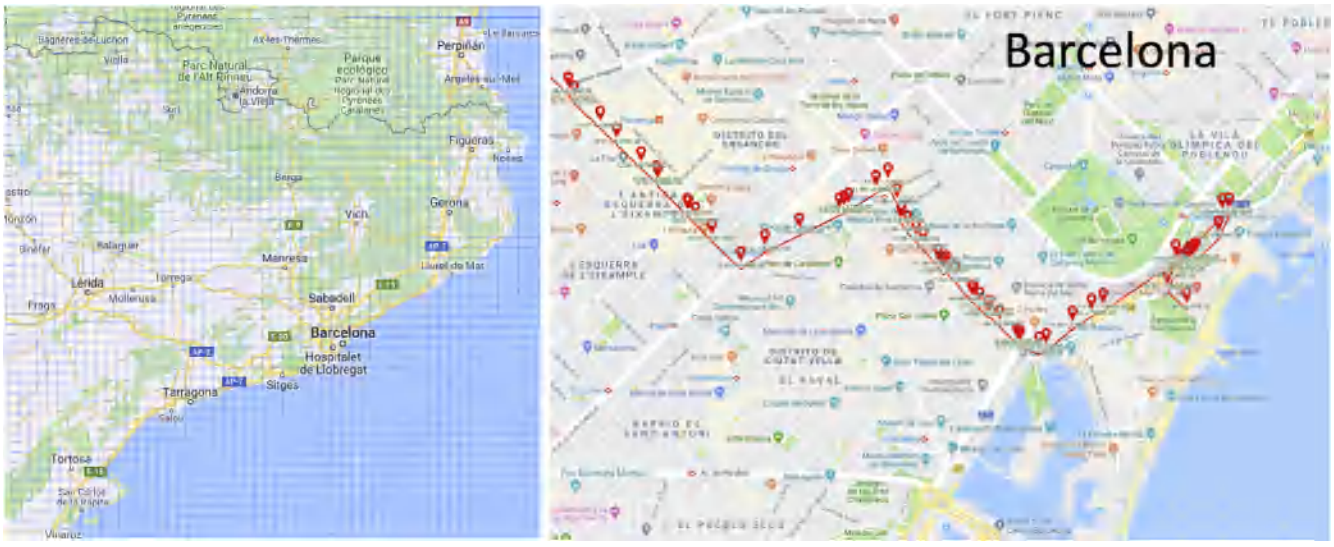

Fig. 6. Map of Catalonia divided in 1425 cells (left). GPS coordinates of some spectra registered in Barcelona (right).

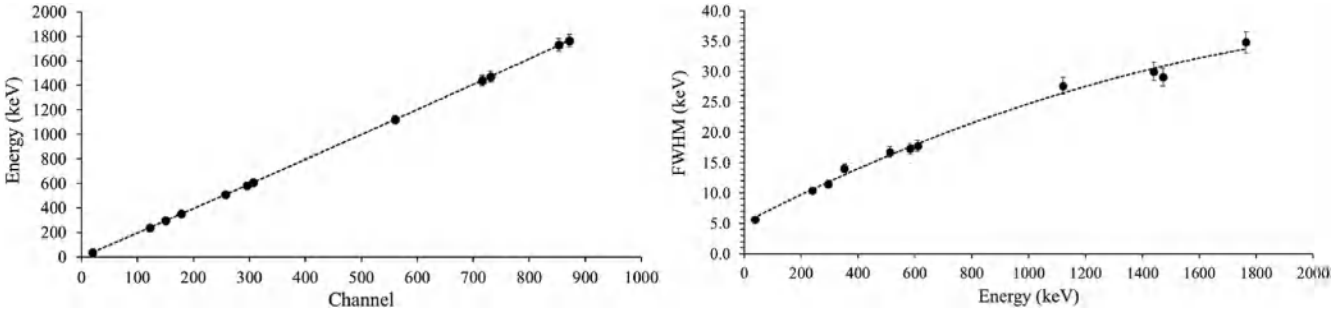

Fig. 8. Energy (left) and resolution (right) calibration curves.

3. Results and discussion

3.1. Energy, resolution and efficiency calibrations

The energy and resolution calibrations provided adequate results that are shown in Fig. 8. We adjusted a 2nd degree polynomial in both cases, obtaining values of r^2 not lower than 0.9999. The spectrum used for the calibration in energy and resolution was equivalent to the spectrum presented in a previous article (Prieto et al., 2018).

Fig. 9 demonstrates the variation of the efficiency values for a monoenergetic homogenous source of 661 keV in function of the size. In both scenarios, the efficiency tends to stabilize when the source size increases. The error bars of the data points represent the statistical uncertainties from the EGS5 calculation (see reference (Casanovas et al., 2012a) for more detail about uncertainty calculations).

The obtained efficiencies are similar to those calculated in a previous study (Casanovas et al., 2014), despite the efficiencies were calculated simulating the detectors mounted on the car structure. The mobile unit attenuates a little amount of gamma rays arising from a homogeneous large source. Therefore, the car structure has not a remarkable effect in the detector efficiencies for large size sources.

Based on these results, the superficial, volumetric and point-like efficiency curves were calculated for 18 different energy sources ranging from 0 to 2000 keV with 2R = 100 m for the superficial geometry and 2R = 300 m (H = 300 m) for the volumetric one. Efficiency values are in the stable zone with uncertainties of less than 9% for this source sizes.

Fig. 10 presents the efficiency curves of the detectors calculated using MC code for superficial, volumetric and a point-like source placed at 5 m from the rear of the mobile unit. In all cases, the higher efficiency is achieved for energies around 200 keV.

A 6-degree polynomial curve (Equation (1)) fitted the efficiency values for all scenarios, obtaining a r^2 coefficient of 0.999 (superficial and point-like) and 0.986 (volumetric). The error bars of the data points represent the statistical uncertainties from the EGS5 calculation (see reference (Casanovas et al., 2012a) for more detail about uncertainty calculations). The lower uncertainties from de data of the superficial and point-like scenarios allow a better fit of the polynomial equation.

Although the simulation for each energy was carried out for 10^8 histories, the computation time ranged from 16 h to 58 h depending on the source size and the energy.

3.2. Attenuation

The attenuation calculated using MC simulations for the volumetric and the superficial source term scenarios obtained an attenuation below 5% for the volumetric source term and of 33% for the superficial one.

The attenuation of a point-like source was obtained experimentally. Fig. 11 indicates the attenuation values in different positions along the longitudinal axis of the car. In order to improve the statistics, we calculated the longitudinal attenuation as the mean value of both detectors. Although the source was only under the car from −0.5 to 4 m, the attenuation increases with the longitudinal axis in all the positions due to the mobile unit's geometry and composition. The position of the source and the sign convention is illustrated in Fig. 5.

The attenuation values for the transversal position were obtained independently for both detectors. The attenuation increases when the source is placed at opposite positions to the detector and decreases at positions located at the same side showing little variations between both detectors. Fig. 12 illustrates the attenuation of the detector placed at the left side of the car (viewed from behind).

The attenuation is nearly constant and has an important effect when detecting a source placed opposed to and under the car. For detector 1, the mean attenuation for positions from −4 to 0.5 m is 0.81 and for detector 2 (from −0.5 to 4 m) is 0.70. This variation can be attributed to the different internal structure of the mobile unit in its laterals, for example, the fuel tank shape and position.

The attenuation of the car affects much less for the detection of a source located on the same side of the detector. For detector 1, the mean attenuation (from 1 to 4 m) is 0.31, whereas for detector 2 (from −4 to −1 m) is 0.15. Thus, the cps registered variate mostly due to the detector – source distance.

The different response of the detectors when a source is placed on the transversal axis of the mobile unit could be useful to detect and

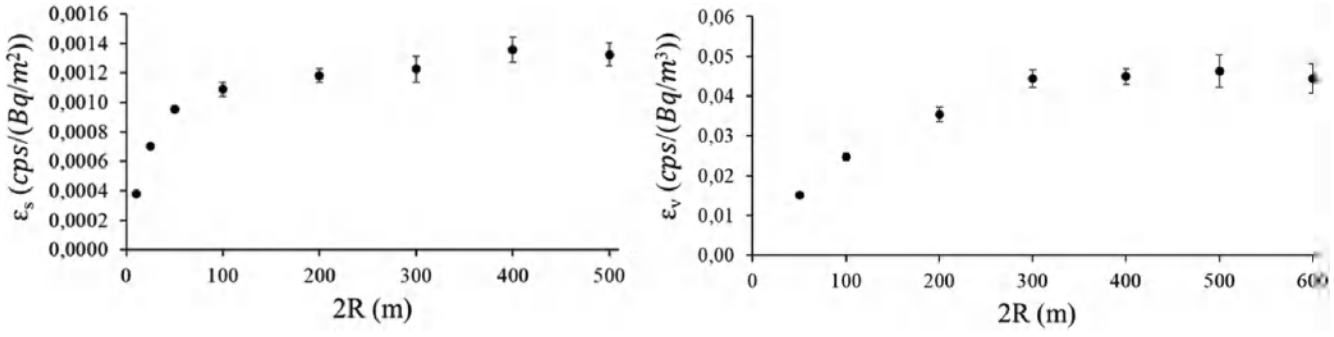

Fig. 9. Superficial (left) and volumetric (right) efficiency values for different source sizes of 661 keV.

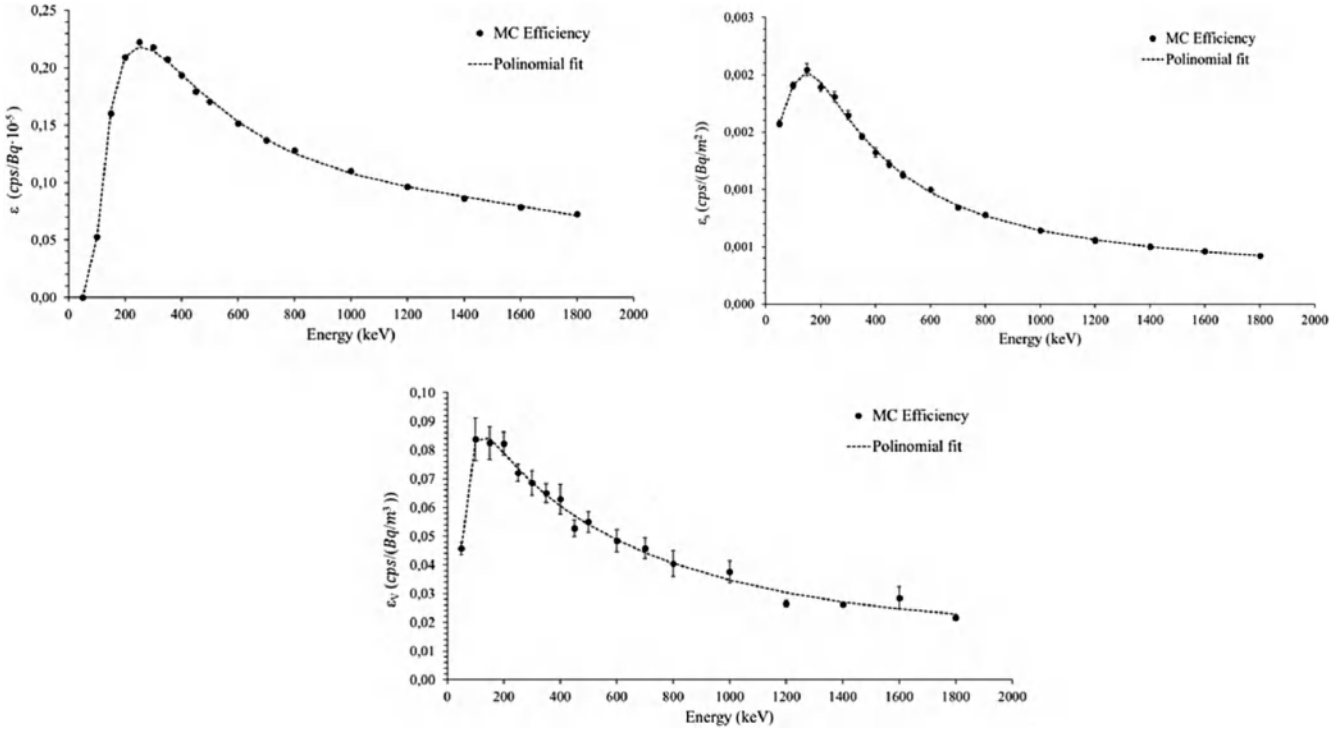

Fig. 10. Point-like source at 5 m (top left), superficial (top right) and volumetric (bottom) efficiency curves calculated with MC code for 18 different homogenous and monoenergetic sources. For some data points, error bars are smaller than the size of the bullet points.

determine the location of a point-like source during normal operation.

3.3. Ambient dose equivalent H*(10)

We compared the H*(10) calculated from the spectra to the H*(10) given by a calibrated proportional counter and to the H*(10) value obtained by TLDs. The mean value obtained from the spectra (0.067 μSv/h) was rescaled to correspond to the measurement of the TLDs (0.078 μSv/h, black line in Fig. 13). The relative variations of the H*(10) obtained from spectra were calibrated to correspond to the relative variations of the proportional counter using a 2nd degree polynomial with a r^2 value of 0.9995. The minimum and maximum values obtained from the spectra were 0.055 μSv/h and 0.081 μSv/h respectively, whereas after the adjustment the values were 0.072 μSv/h and 0.088 μSv/h. After the rescale and calibration, the measurement of H*(10) from spectra was in agreement with those of the proportional counter and the TLDs.

3.4. Spectral windows or ROIs

The spectral windows method obtained the activity concentration of some isotopes for the different geometries considered in the efficiency curves. By way of example, the activity concentration for the volumetric efficiency of ^{214}Bi is shown in Fig. 14. The values of the activity concentration of ^{214}Bi variate due to the characteristics of the different geographical locations (soil composition, radon emanation rates, etc.) where the measurements were registered. The mobile unit measured spectra only in similar and favourable weather conditions to minimise natural fluctuations caused by the meteorological variables such as the precipitation or humidity variations.

The activity concentration of ^{137}Cs fluctuates around 0 in all measurements. However, to show the system response on anthropogenic isotopes, we provide results for a ^{137}Cs point-like source placed at 5 m from the rear of the mobile unit in Fig. 15. This exposure is also treated as if it were due to a volumetric and a superficial source of ^{137}Cs. The exposure to ^{137}Cs triggered the statistical criterion ($\bar{x} + 3.5\sigma$) for all source geometry assumptions. All the activity concentrations are also

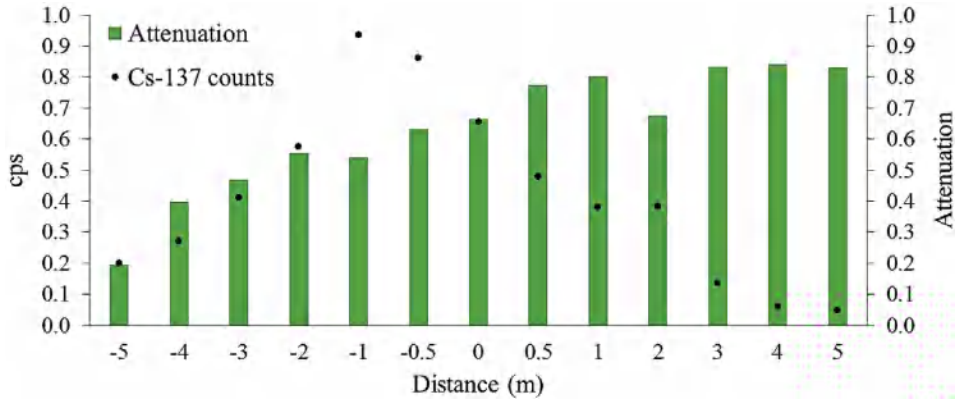

Fig. 11. Attenuation and ^{137}Cs cps values in several positions along the longitudinal axis of the mobile unit.

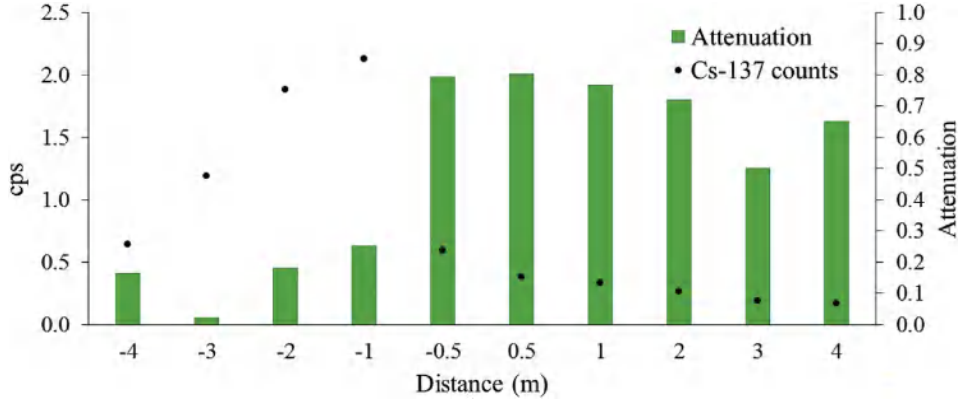

Fig. 12. Attenuation and ^{137}Cs counts values from detector 2 in several positions of the transversal axis of the mobile unit.

related to the increment of the ambient dose equivalent H*(10) that the ^{137}Cs produces when there is a positive detection.

Thus, Fig. 15 presents a set of measurements of ^{137}Cs obtained from environmental spectra (measurements from 0 to 1000) and from spectra registered with a ^{137}Cs point-like source (measurements from 1000 to 1200). Three axis illustrate the activity concentration that would have been obtained considering three different situations: a point-like source at 5 m from the rear of the mobile unit, a superficial source term and a volumetric source term. The figure also shows the increment to the ambient dose equivalent produced by a ^{137}Cs detection.

The amount of the ambient dose equivalent due the ^{137}Cs activity concentration is the same for the different source geometries as it is related to the number of impacts on the detector crystal independently of the source term distribution.

3.5. MDAC

To provide some values related to the measurement capabilities of the mobile unit, the minimum detectable activity concentration was calculated for ^{137}Cs and for ^{131}I for the volumetric and superficial source distributions. Besides, the minimum detectable activity for a point-like source at 5 m was also calculated.

The MDACs presented in Table 1 are affected by the low values of the efficiency curves and the low time of measurement set at 30 s. The low time of measurement generates high MDAC values, as the mobile unit's objective is to obtain fast measurements. These fast measurements provide a low amount of data to obtain good statistics. If lower MDACs were required, integration times could be increased. The results are of the same order as the discrimination criterion ($\bar{x} + 3.5\sigma$). Thus, both thresholds can be used as an alarm trigger.

In situations where an infinite volumetric or superficial source is assumed, the cps of the spectra registered in each detector could be added and thus, the MDAC could be lowered. However, if a source were detected by only one of the detectors, adding the two spectra would decrease the number of cps associated to the detected source and the capabilities of the analysis methods would be worsened.

3.6. Real detection example

To show the feasibility of the system and its potential for future applications in radiation monitoring during nuclear emergencies, we also provide an example of an unexpected real detection of anthropogenic isotopes that occurred during the validation phase of the equipment.

During routine measurements, the mobile unit detected an increment of 65 nSv/h above the background level (70 nSv/h) during 2 min. After a thorough analysis of the situation, the increment was found to be due to the presence of ^{192}Ir, which was being used in a construction site on the road. The use of this radionuclide was controlled, had been previously notified to the safety authorities and did not suppose a risk to the population.

^{192}Ir is a radioactive isotope that emits gamma rays of several energies. The emissions with probabilities higher of 10% are 316.51 keV (82.85%), 468.07 keV (47.84%), 308.46 keV (29.7%) and 295.86 keV (28.71%). This isotope is frequently used for industrial radiography and

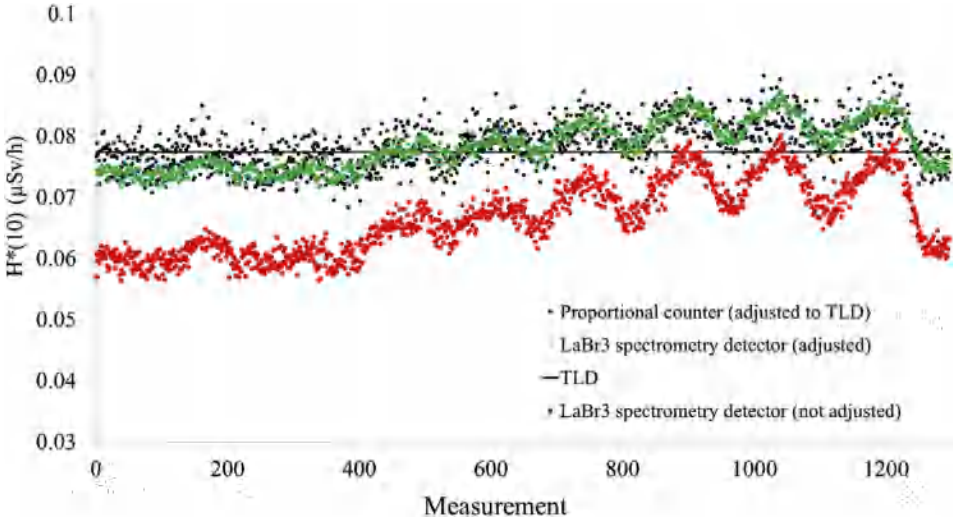

Fig. 13. The obtained H*(10) from a $LaBr_3$ detector (red dots) was adjusted to the H*(10) measurements of a proportional counter (black dots) and of the TLDs (black line). The result is illustrated in green dots. (For interpretation of the references to colour in this figure legend, the reader is referred to the Web version of this article.)

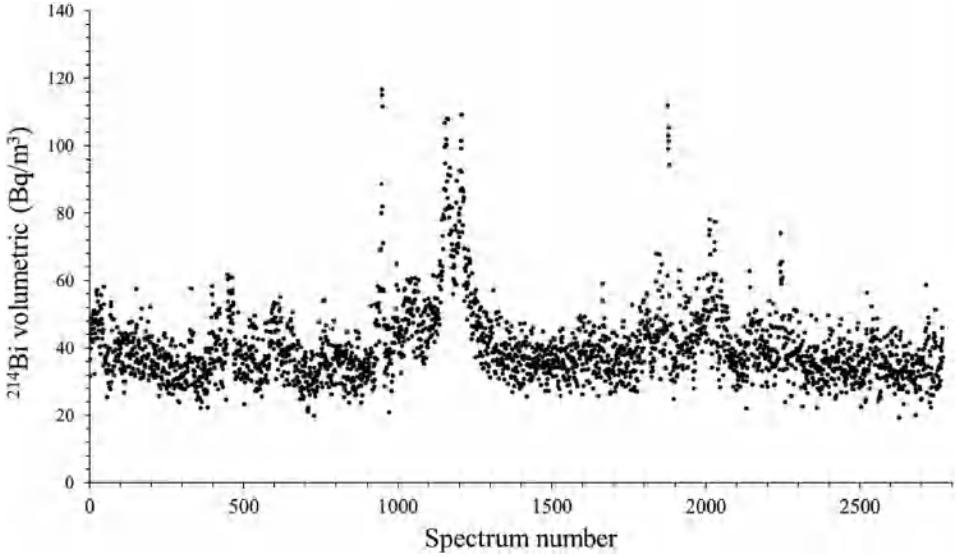

Fig. 14. Activity concentration of ^{214}Bi calculated using the spectral windows method for a volumetric source term.

non-destructing testing.

Fig. 16 presents the spectrum registered during the detection of the ^{192}Ir source. The black line shows the net counts after the subtraction of the $LaBr_3$(Ce) self-activity spectrum. We identified and tagged peaks from ^{192}Ir, even if they are not well defined. The location of the source in contact with the ground causes the high Compton scattering present in the spectrum.

4. Conclusions

A mobile unit using $LaBr_3$(Ce) scintillation detectors has been set up and it is ready for radiological measurements. The set up included detector calibrations (energy, resolution and efficiency), implementation of analytical methods to obtain H*(10) and activity concentrations, calculation of MDAC values and the development of a software to acquire and analyse data.

The system is able to monitor H*(10) and to provide activity concentrations of the different isotopes. Thus, it permits to detect and analyse small fluctuations of anthropogenic isotopes and to distinguish them from those from natural origin. When precise activity concentrations are needed, efficiency calculations can be adjusted to the exact source term geometry, allowing us to evaluate the activity concentrations more realistically.

Table 1
MDAC/MDA and $\bar{x} + 3.5\sigma$ values for three source term geometries of ^{137}Cs and ^{131}I. Calculations were performed for one detector with an integration time of 30 s.

	Volumetric (Bq/m^3)		Superficial (Bq/m^2)		Point-like at 5 m (MBq)	
	MDAC	$\bar{x} + 3.5\sigma$	MDAC	$\bar{x} + 3.5\sigma$	MDA	$\bar{x} + 3.5\sigma$
^{137}Cs	25.5	25.4	1300	1296	0.82	0.81
^{131}I	19.5	21.8	861	965	0.61	0.68

The capabilities of the mobile unit monitoring system were determined by calculating the MDAC values. High MDAC values were obtained due to short integration times (30 s). The short measurements of the mobile unit aim to be a representation of a small area since they

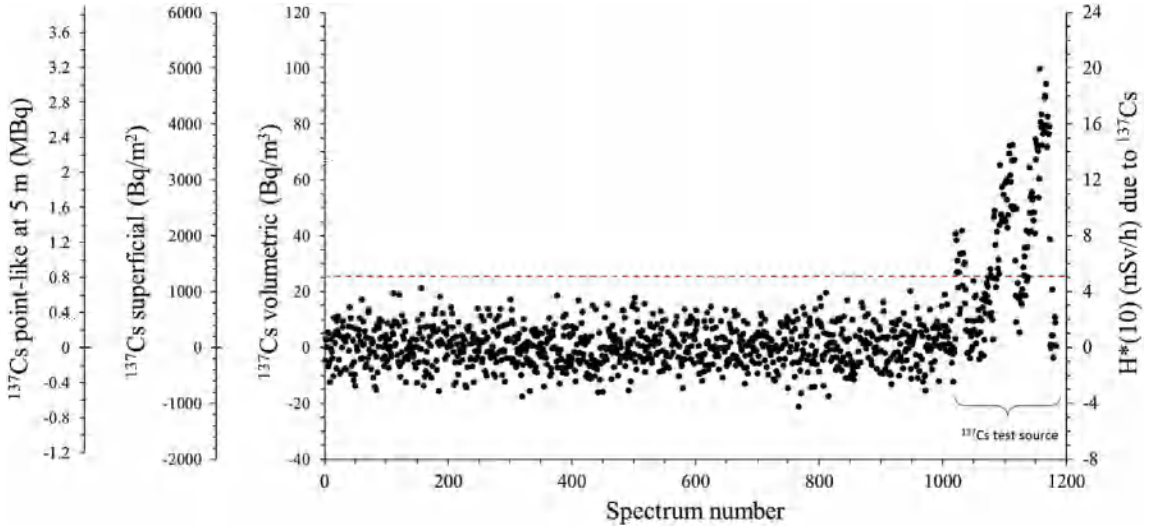

Fig. 15. Activity concentrations and the associated increment to the ambient dose equivalent of ^{137}Cs. The first axis on the left corresponds to a point-like source at 5 m from the rear of the mobile unit, the second corresponds to a superficial source term and the third corresponds to a volumetric source term. The axis on the right presents the increment of the ambient dose equivalent produced by ^{137}Cs. The dotted line (red colour) represents the $\bar{x} + 3.5\sigma$ criterion. (For interpretation of the references to colour in this figure legend, the reader is referred to the Web version of this article.)

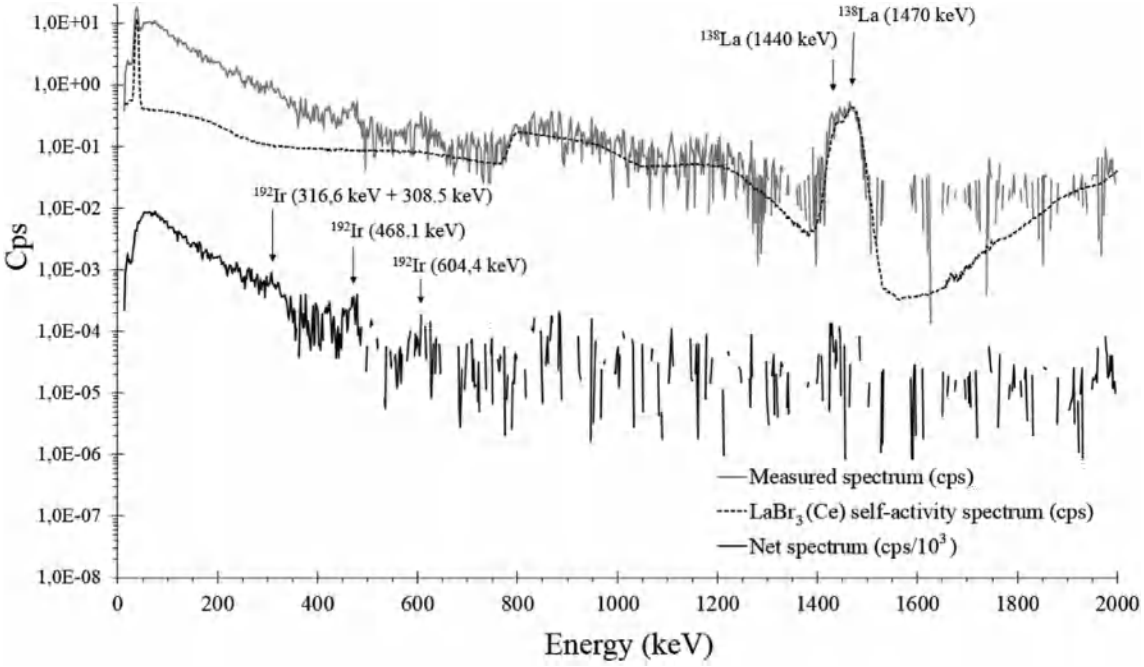

Fig. 16. Detection of a ^{192}Ir source during an integration time of 2 min in a construction site. The gray line corresponds to the measured spectrum, the dotted line corresponds to the background self-activity spectrum of the $LaBr_3$(Ce) crystal and the black line is the net spectrum, where the peaks from ^{192}Ir can be identified.

are registered when the car is in motion. However, if necessary, higher integration times could be used to obtain lower MDACs.

The mobile unit was tested on the field and provided good results. Therefore, it is ready to be used for measuring radiological data of large areas, either for routine measurements or during a nuclear emergency. In particular, this mobile unit will acquire spectra to create a radiological map of Catalonia.

To do so, the mobile unit will collect and analyse data during the following months. We will obtain information about the natural radiological state of the region. The collected information will allow us to determine the areas of special interest due to natural or even anthropogenic radionuclides, if detected. These areas will be studied thoroughly in the last phase of the project.

Declaration of competing interest

The authors declare that they have no known competing financial interests or personal relationships that could have appeared to influence the work reported in this paper.

References

Baeza, A., Corbacho, J.A., Miranda, J., 2013. Design and implementation of a mobile radiological emergency unit integrated in a radiation monitoring network. IEEE Trans. Nucl. Sci.

Berger, M., Coursey, J., Zucker, M., Chang, J., 2005. ESTAR, PSTAR, and ASTAR: Computer Programs for Calculating Stopping-Power and Range Tables for Electrons, Protons, and Helium Ions (Version 1.2.3) [Internet]. National Institute of Standards and Technology, Gaithersburg Available from: https://www.nist.gov/pml/stopping-power-range-tables-electrons-protons-and-helium-ions.

Casanovas, R., Morant, J.J., Salvadó, M., 2012a. Energy and resolution calibration of NaI (Tl) and LaBr 3(Ce) scintillators and validation of an EGS5 Monte Carlo user code for efficiency calculations. Nucl. Instrum. Methods Phys. Res. Sect. A Accel. Spectrom. Detect. Assoc. Equip. 675, 78–83.

Casanovas, R., Morant, J.J., Salvadó, M., 2012 Augb. Temperature peak-shift correction methods for NaI(Tl) and LaBr3(Ce) gamma-ray spectrum stabilisation. Radiat. Meas. 47 (8), 588–595.

Casanovas, R., Morant, J.J., Salvadó, M., 2014. Development and calibration of a real-time airborne radioactivity monitor using direct gamma-ray spectrometry with two scintillation detectors. Appl. Radiat. Isot. 89, 102–108.

Casanovas, R., Prieto, E., Salvadó, M., 2016. Calculation of the ambient dose equivalent H*(10) from gamma-ray spectra obtained with scintillation detectors. Appl. Radiat. Isot. 118, 154–159.

Currie, L.a., 1968. Limits for qualitative detection and quantitative determination. Application to radiochemistry. Anal. Chem. 40 (3), 586–593.

ICRP: ICRP Publication 103, 2007. The 2007 recommendations of the international commission on radiological protection. Ann. ICRP.

ICRU: ICRU Report 39. Determination of Dose Equivalents Resulting from External Radiation Sources.

Kock, P., 2010. Orphan source detection in mobile gamma-ray spectrometry. In: Nuclear and Radiological Emergencies and Incidents.

Prieto, E., Casanovas, R., Salvadó, M., 2017. Spectral windows analysis method for monitoring anthropogenic radionuclides in real-time environmental gamma-ray scintillation spectrometry. J. Radiol. Prot. 38 (1), 0–48.

Prieto, E., Casanovas, R., Salvadó, M., 2018. Calibration and performance of a real-time gamma-ray spectrometry water monitor using a LaBr3(Ce) detector. Radiat. Phys. Chem. 144.

Takeishi, M., Shibamichi, M., Malins, A., Kurikami, H., Murakami, M., Saegusa, J., et al., 2017. Using two detectors concurrently to monitor ambient dose equivalent rates in vehicle surveys of radiocesium contaminated land. J. Environ. Radioact.